

## Simulation of temperature distribution in ship structures for the determination of temperature-dependent material properties

Jan M. Kubiczek<sup>1</sup>, Hauke Herrnring<sup>1</sup>, Leon Kellner<sup>1</sup>, Sören Ehlers<sup>1</sup>, Roman Diewald

<sup>1</sup>Hamburg University of Technology

### 1 Introduction

Several Arctic waters are no longer ice-covered throughout the year. As a result, the Northern Sea Routes are getting into the focus of the maritime industry [1]. In addition less ice coverage in other sea areas such as the Baltic Sea leads to increased shipping traffic in the winter season. This repeatedly leads to damages to ships when sailing in ice-covered waters, but also when colliding with ice floes and icebergs but also with ships, such as icebreakers, in convoys [2, 3].

It is of great importance for the structural simulation of these events to model the material properties of the ship structure under consideration of the environmental conditions. These material properties such as yield strength and tensile strength as well as fracture strain, however, are strongly influenced by the material temperature [4]. Therefore the question arises how cold a ship structure can actually become in winter and in arctic waters and how this affects the structural response in the event of a collision.

In the rules and guidelines of the classification societies -60 °C can be found as the lowest temperature for material tests on steels used in shipbuilding [5]. This value corresponds well with different temperature measurements where extreme values below -50 °C were measured in the area of the Northern Sea Route [6, 7]. In contrast, liquid seawater cannot become colder than -2 °C [8]. If the interaction with ice is considered, the structural temperature in the waterline area is of particular interest. It is influenced by both water and air temperature.

Therefore, the structure temperature is estimated by thermal simulations in order to determine suitable temperature depended material curves and to predict the influence on the structural response in the collision scenario.

### 2 Collision scenario

It is well known that high loads on a ship's hull may occur by ramming ice floes while sailing in a broken ice field, see [9] and [10]. That is why it is necessary to find an approach for loads induced by ice floes. In a broken ice field, a ship might reach a higher speed than in level ice. Thus the energy introduced in the collision with the ice floe is much higher. In this load scenario it is assumed that the ship's speed does not decrease because of the ramming of the ice floe. The encounter speed is the difference of the ship's and the floe's speed.

$$v_{encounter} = v_{Ship} - v_{floe} \quad (1)$$

For this load scenario it is assumed that there is neither wind nor current, so that the speed of the ice floe is zero. Since the ship's speed is assumed to remain constant in the moment of the collision, the ship's momentum  $P_{Ship}$  is constant.

$$P_{Ship} = m_{Ship} \times v_{Ship} \quad (2)$$

$m_{Ship}$  is the ship's mass and  $v_{Ship}$  its velocity. The ship's velocity can be estimated based on the *Polar Operational Limit Assessment Risk Indexing System* (POLARIS) [11] introduced by the *International Association of Classification Societies* (IACS) as given in the following table.

Table 1: Table 1: POLARIS speed limitations

Ice Class	Speed limit [kn]
PC1	11
PC 2	8
PC3 – PC 5	5
PC6 – PC 7	3
IA Super – IA	NA
Below IA	NA

During the collision, the ice floe is accelerated to the velocity of the ship. The change of its momentum during the collision is the product of its mass and the encounter speed:

$$\frac{dP_{floe}}{dt} = \frac{(m_{floe} + m_{hydro}) \times v_{encounter}}{dt} = F_{ext} \quad (3)$$

According to the momentum equation [12] the change of the momentum over time is equal to the sum of all external forces  $F_{ext}$ . The external forces can only be transferred to the ship's hull (the energy transferred to the water by radiation is neglected). The parameter  $m_{floe}$  represents the mass of the ice floe and  $m_{hydro}$  represents the hydrodynamic mass of the ice floe. If we idealize the ice floe as a round disc, the mass can be determined as follows:

$$m_{floe} = \pi \cdot \rho_{ice} \cdot \left(\frac{d}{2}\right)^2 \cdot h \quad (4)$$

$\rho_{ice}$  is the density of the ice flow,  $d$  is the diameter and  $h$  is the thickness. The hydrodynamic added mass per unit length  $m''$  is given in [13] as follows:

$$m'' = \pi \cdot \rho_{fluid} \cdot \left(\frac{d}{2}\right)^2 \quad (5)$$

This value has to be multiplied by the draft of the ice floe to obtain its hydrodynamic mass  $m_{hydro}$ . The estimation of the diameter of the ice floe is somewhat difficult. Since the break-up and refreezing of ice is a random process, no exact values can be obtained for the dimensions of an ice floe. Nevertheless, there have been analyses aiming on providing statistics about the size of ice floes [14–17]. The common conclusion is that the cumulative number of floes having a certain diameter,  $N(d)$ , follows a power-law distribution:

$$N(d) = \beta \times d_{floe}^{-\alpha} \quad (6)$$

where  $\beta$  is a factor depending on the total number of observed floes. It is required to get the exact number of floes having a certain diameter. Nevertheless,  $\beta$  does not affect the cumulative number distribution itself. That is why it is set to 1 in the following.

Some of the values found for  $\alpha$  are given in Table 2. Some of the studies mentioned above indicate that  $\alpha$  changes for higher diameters, e.g. more than about 30 meters. Since for the collision event only smaller floes are of interest,  $\alpha$  is given for smaller diameters only.

Table 2:  $\alpha$ -values for different sea areas

Sea Area	Year	$\alpha$
South Okhotsk Sea	2003	1.15
Wedell Sea 1	2006	1.39
Wedell Sea 2	2006	1.2
Wedell Sea 3	2006	1.05
Off Wilkes Land 1	2007	1.52
Off Wilkes Land 2	2007	1.26
Off Wilkes Land 3	2007	1.03
Beaufort Sea 1	1998	2.013
Beaufort Sea 2	1998	2.013
Beaufort Sea 3	1998	2.018
Beaufort Sea 4	1998	2.031
Beaufort Sea 5	1998	2.023
Beaufort Sea 6	1998	2.03
Beaufort Sea 7	1998	2.033
Beaufort Sea 8	1998	2.144
Beaufort Sea 9	1998	2.178
Beaufort Sea 10	1998	2.079

In Figure 1 an example for a cumulative number distribution is given for  $\alpha = 1.23$  being the mean value of the first seven entries in Table 2.  $N(d)$  is less than 0.01 for a diameter greater than 42.5 m. Thus, this value might be assumed as an upper threshold for the diameters under consideration. Following Pareto's Principle, 80 % of all occurring floes have a diameter of maximum 20 % of the upper boundary value, e.g.  $d_{80} = 0.2 \times 42.5 \text{ m} = 8.5 \text{ m}$ . This value can serve as an upper boundary value for

the estimation of the mass of a floe. Of course, it strongly depends on the selection of the parameter  $\alpha$ , so attention must be paid to this topic.

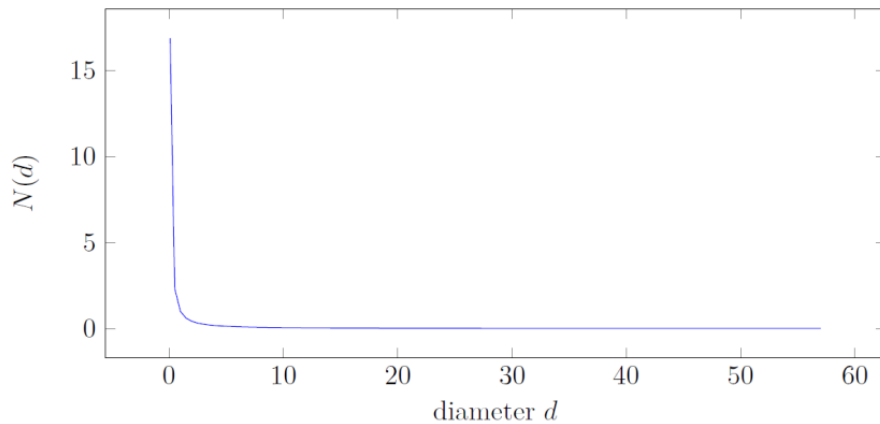


Fig.1: Example cumulative number distribution

The next parameter needed for the estimation of the mass of a floe is the density of ice. Since ice is a natural product, its density varies over a wide range [18]. Here, a value of  $\rho_{ice} = 0.91 \text{ t/m}^3$  is chosen. Naturally, an ice floe is covered with snow, which influences the density of the ice-snow-compound. This is also neglected here.

The last value needed for the calculation of the floe's mass is the ice thickness. This is estimated with  $h = 0.8 \text{ m}$  according to [19] for ice class IA. Since ice usually breaks up when the temperature rises, one should be aware that melting continuously reduces the thickness of the ice. Nevertheless, the lateral melting from the edges is considered to be more decisive than melting from top or bottom [14]. With the values obtained above, the total mass of the ice floe can be estimated as follows:

$$m_{total} = m_{floe} + m_{hydro} = \pi \cdot \frac{0.91 \text{ t}}{\text{m}^3} \cdot \left(\frac{8.5 \text{ m}}{2}\right)^2 \cdot 0.8 \text{ m} + \pi \cdot \frac{1.024 \text{ t}}{\text{m}^3} \cdot \left(\frac{8.5 \text{ m}}{2}\right)^2 \cdot 0.71 \text{ m} = 82.6 \text{ t} \quad (7)$$

The ship examined is a container ship comparable to the ship „FORESIGHT” that transited the Northern Sea Route in 2009 classified as IA. Since this is equivalent to PC7, a ship speed of 3 knots is assumed. This corresponds to about 1.543 m/s. The main dimensions are listed in Table 3.

Table 3: Main dimensions and environmental conditions

<b>Ice class:</b>	FSICR IA (equivalent to PC7)
<b>Length:</b>	134.4 m
<b>Beam:</b>	22.5 m
<b>Draught:</b>	8.08 m
<b>Engine:</b>	8400.0 kW
<b>Ship speed:</b>	1.543 m/s
<b>Wind and Current speeds:</b>	0 m/s

The used FE model, shown in Figure 2, is a 8.4 m long section of the ship's structure on half the length of the ship, modelled with shell elements. The ship structure is supported at all free edges with appropriate boundary conditions. The ice floe has an initial velocity perpendicular to the ship's hull but is otherwise not guided.

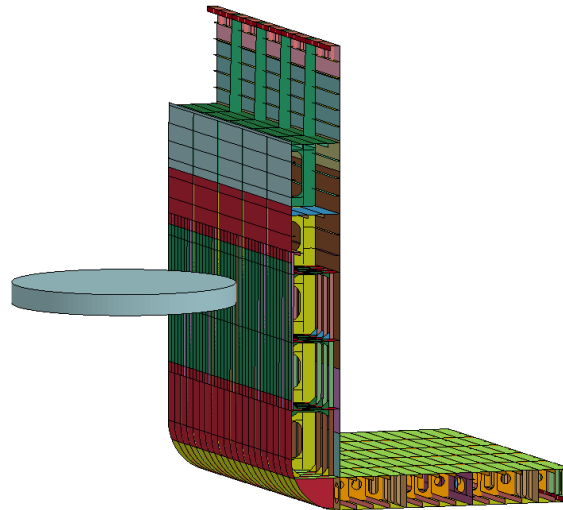


Fig.2: Finite elements Model of the collision scenario

### 3 Estimation of temperature distribution

For the determination of the temperature distribution, a thermal nonlinear analysis is performed assuming that the temperature distribution is stationary, since ships often operate in the same operating state for a longer period of time. The heat transfer is realized by thermal boundary conditions and a corresponding material model. In doing so, the heat transfer by convection and radiation as well as heat conduction is taken into account.

Figure 3 shows the cross-section of the structure under consideration, the different ambient temperatures for the individual areas and the distribution of the thermal boundary conditions.

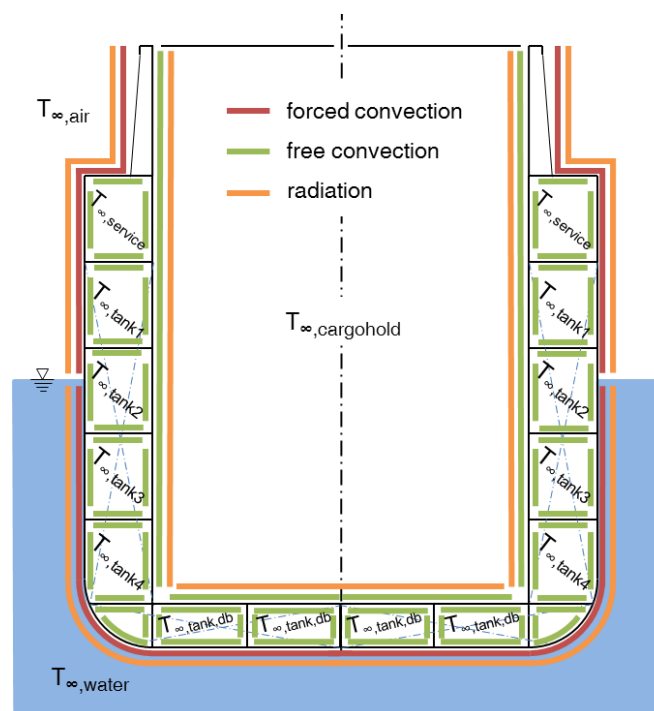


Fig.3: heat transfer assumptions

For heat transfer due to convection, a distinction is made between forced convection due to external influences such as forced movements such as the movement of the ship through water or air and free convection due to, for example, temperature-induced density differences and the associated buoyancy forces within a fluid. Heat transfer due to forced convection is assumed in the ambient water and air flowing along the outer shell and free convection is assumed for the service corridor, in the tanks and in the cargo hold.

A convection boundary condition is used to take this into account. The corresponding heat flow can generally be determined according to [20] as follows:

$$\dot{q}'' = h \cdot (T_{surface} - T_{\infty}) \quad (8)$$

with the heat transfer coefficient  $h$  and the temperature potential between the surface temperature of the structure and the ambient temperature ( $T_{surface} - T_{\infty}$ ). The heat transfer coefficient can be determined as a function of the Nusselt number  $Nu$ , the corresponding length  $l$  and the heat conduction coefficient of the fluid  $\lambda_{fluid}$  according to [21] as follows:

$$h = \frac{Nu \cdot \lambda_{fluid}}{l} \quad (9)$$

While the corresponding length depends on the geometry under consideration only and the heat conduction coefficient is a temperature-dependent material quantity, the differences between forced and free convection as well as the shape of the inflow surface must be taken into account when determining the Nusselt number.

In the case of forced convection, the Nusselt number for a turbulently overflown plane plate can be calculated in dependence of the Reynolds number  $Re_x$  and the Prandtl number  $Pr$  according to [22] as follows:

$$Nu = f(Re_x, Pr) = 0.0296 \cdot Re_x^{\frac{4}{5}} \cdot Pr^{\frac{1}{3}} \quad (10)$$

In the case of free convection, the Nusselt number is a function of the Grashof number  $Gr$  and the Prandtl number  $Pr$  according to [21]:

$$Nu = f(Gr, Pr) \quad (11)$$

When determining the Nusselt number, a distinction must be made between vertically and horizontally oriented surfaces.

For vertical surfaces according to [21] the following applies:

$$Nu = \left[ 8.825 + 0.387 \cdot (Gr \cdot Pr \cdot f_1(Pr))^{\frac{1}{6}} \right]^2 \quad \text{mit } f_1(Pr) = \left[ 1 + \left( \frac{0.492}{Pr} \right)^{\frac{9}{16}} \right]^{-\frac{16}{9}} \quad (12)$$

In the case of horizontally oriented surfaces, a distinction must also be made between heat dissipation to or from the top or bottom.

For heat dissipation at the top or cooling at the bottom the following applies according to [21]:

$$Nu = 0.15 \cdot [Gr \cdot f_2(Pr)]^{\frac{1}{3}} \quad \text{mit } f_2(Pr) = \left[ 1 + \left( \frac{0.322}{Pr} \right)^{\frac{11}{20}} \right]^{-\frac{20}{11}} \quad (13)$$

For heat dissipation at the bottom and cooling at the top the following applies according to [21]:

$$Nu = 0.6 \cdot [Gr \cdot f_1(Pr)]^{\frac{1}{5}} \quad \text{mit } f_1(Pr) = \left[ 1 + \left( \frac{0.492}{Pr} \right)^{\frac{9}{16}} \right]^{-\frac{16}{9}} \quad (14)$$

In addition, due to the expected temperature difference between the ship's structure and its surroundings, heat transfer by radiation is also expected. A radiation boundary condition is used to take this into account. The corresponding heat flow can be determined according to [20] as follows:

$$\dot{q}'' = h_r (T_{surface}^4 - T_{\infty}^4) \quad (15)$$

$h_r$  is the heat transfer coefficient which, according to the following relationship

$$h_r = \sigma \cdot \epsilon \cdot F \quad (16)$$

depends on the Stefan Boltzmann constant  $\sigma$ , the surface emissivity  $\epsilon$  and the surface view factor  $F$ . For this study, the surface emissivity and the surface view factor are estimated to be one. A possible heat transfer by radiation within the structure is neglected at this point.

Furthermore an isotropic material behaviour (**\*MAT\_THERMAL\_ISOTROPIC**) is assumed for the simulation of heat conduction in the steel ship structure. All material values required for the calculations were taken from [22] and [21]. The necessary material data for air, water and steel are defined as **\*DEFINE\_FUNCTION\_TABULATED** as a function of the temperature and the calculation of the heat transfer coefficients and the unitless numbers required for this, such as Grashof number or Prandtl number, is carried out via **\*DEFINE\_FUNCTION**, since these are dependent not only on the ambient temperature but also on the unknown structural temperature, whereby an iterative solution is required.

As shown in Figure 3 the ship consists of a side double hull, a double bottom and a large hold in the area under investigation. In the area of the side double hull on port and starboard, the ship has a service corridor with the ambient temperature  $T_{\infty,service}$ . Three thermal load cases are conceivable for this area, depending on the use:

- the area is heated to 5 °C to prevent ice formation.
- in this area a complete air exchange takes place at least twice an hour, so that the outside temperature  $T_{\infty,air}$  can be set here
- the air temperature is unknown and will adjust according to the temperatures of the surrounding surfaces

Below the service corridor there is a side tank, which is divided into 4 individual compartments (Tank1-4) with the ambient temperatures  $T_{\infty,tank1-4}$  in this study. Two thermal load cases are conceivable for this area:

- the tank is filled and heated to 5 °C to prevent ice formation.
- the tank is empty and the air temperature is unknown. In this case, it is to be expected that the temperature will adjust according to the temperatures of the surrounding surfaces.

The double bottom is also designed as a tank, with the temperature  $T_{\infty,tank,db}$ . It is assumed that this tank is always filled and heated to 5 °C to prevent ice formation.

A complete air exchange can be assumed for the hold at least twice an hour, so that the ambient temperature  $T_{\infty,cargohold}$  can be set to the outside temperature  $T_{\infty,air}$ .

All in all these considerations result in six relevant thermal load scenarios, which are shown in Table 4:

Table 4: Temperature definitions of load cases for thermal analyses

Load case	Tanks	Service way $T_{\infty,Service}$	Cargohold $T_{\infty,cargohold}$	Ambient Air $T_{\infty,air}$	Ambient Water $T_{\infty,water}$
LCa	full : $T_{\infty,tank1-4}=5\text{ °C}$ full : $T_{\infty,tank,db}=5\text{ °C}$	?	-60 °C	-60 °C	0 °C
LCb	full : $T_{\infty,tank1-4}=5\text{ °C}$ full : $T_{\infty,tank,db}=5\text{ °C}$	-60 °C			
LCc	full : $T_{\infty,tank1-4}=5\text{ °C}$ full : $T_{\infty,tank,db}=5\text{ °C}$	5 °C			
LCd	empty : $T_{\infty,tank1-4}=?$ full : $T_{\infty,tank,db}=5\text{ °C}$	?			
LCe	empty : $T_{\infty,tank1-4}=?$ full : $T_{\infty,tank,db}=5\text{ °C}$	-60 °C			
LCf	empty : $T_{\infty,tank1-4}=?$ full : $T_{\infty,tank,db}=5\text{ °C}$	5 °C			

## 4 Material Modelling

### 4.1 Steel material model

The ship's structure is constructed of bulb flat profile reinforced plate sections made of a DH36 steel with a nominal yield strength of 355 N/mm<sup>2</sup>. The plates and the webs of the profiles are idealised with

shell elements and the bulbs of the profiles with beam elements. For the simulation **\*MAT123** is used for the shell elements and **\*MAT24** for the beam elements. Material curves used to describe the plastic material behaviour are based on the quasi static tensile test results shown in Figure 4, which were determined by [4].

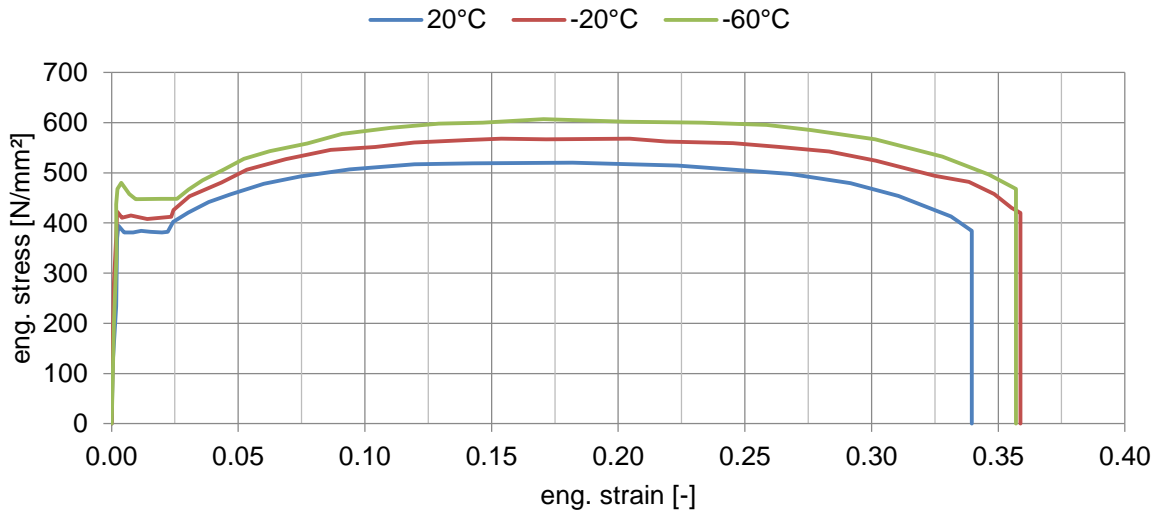


Fig.4: Engineering stress strain curves for a DH36 steel [4]

For this purpose, the obtained technical stress strain curves are converted into true effective stress and true effective strain curves assuming a constant volume up to tensile strength [23]. Subsequently, with the method presented by [24] the further curve gradient until failure is optimized on the basis of finite element simulations of the corresponding tensile tests in order to achieve the best possible agreement between simulation and measured data.

#### 4.2 Ice material model

A pragmatic approach was chosen for the ice material model enabling deformations of the ice floe and to avoid hard points at the edges as they can occur in collisions with rigid bodies. A simple isotropic elastic perfectly plastic material model was applied, which assumes a homogeneous bulk response (**\*MAT\_PLASTIC\_KINEMATIC**). The elastic parameters and the density were taken as  $E = 9 \text{ GPa}$ ,  $\nu = 0.33$ ,  $\rho_{\text{ice}} = 0.91 \text{ tm}^{-3}$  from [18, 25], respectively. Plasticity was added to avoid unphysical stress peaks where corners or edges of the ice floe come into contact with the steel structure. Plasticity for ice impact modeling is often combined with yield surfaces, since the yield stress depends on hydrostatic pressure, e.g. [26]. Here, the highest possible yield stress was used instead of a yield surface. The highest yield stress was taken from [26] and [27], respectively, as the apex of a yield surface recommended for “[...] the local deformation of ship structure during ice impacts” [26, p. 329]. Hence, the yield surface is given as

$$f(p, J_2) = J_2 - (a_0 + a_1 p + a_2 p^2) = 0 \quad (17)$$

where  $p$  is pressure and  $J_2$  the second invariant of the deviatoric stress tensor. With fitting values  $a_0 = 22.93 \text{ MPa}$ ,  $a_1 = 2.06$ ,  $a_2 = 22.93 \text{ MPa}^{-1}$  the maximum values for  $p$  and  $J_2$  are  $p_{\text{max}} = 45 \text{ MPa}$ ,  $J_{2\text{max}} = 70 \text{ MPa}$ . Finally, the maximum v. Mises yield stress is obtained as

$$\sigma_{\text{yield},vM} = \sqrt{3J_2} = 14.5 \text{ MPa} \quad (18)$$

### 5 Results and Discussion

Before calculating the temperature distribution in the ship’s structure, the unknown ambient temperatures in the service corridor and in the empty tank compartments 1 to 4 need to be determined. For this purpose it is assumed that the mean ambient temperature in a room corresponds approximately to the mean value of the temperature of all surrounding surfaces. With this assumption, the unknown temperatures can be determined iteratively as shown in Figure 5. The starting value is the temperature of the outside air  $T_{\infty,air}$  and a stable equilibrium can be achieved within 10 iterations for each load case.

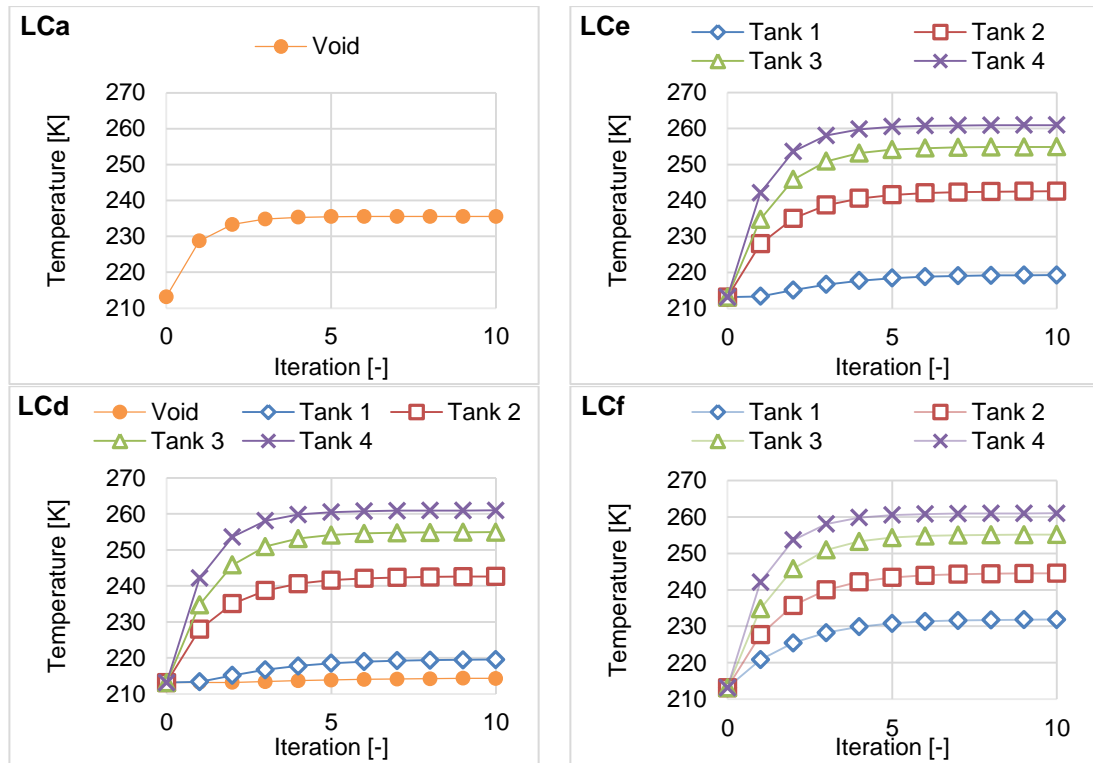


Fig.5: Iterative determination of unknown temperatures in the service corridor and empty tank compartments

Now the temperature of the outer hull can be determined for all load cases in the next step. Figure 6 shows the temperature distributions for the three load cases with filled side tank.

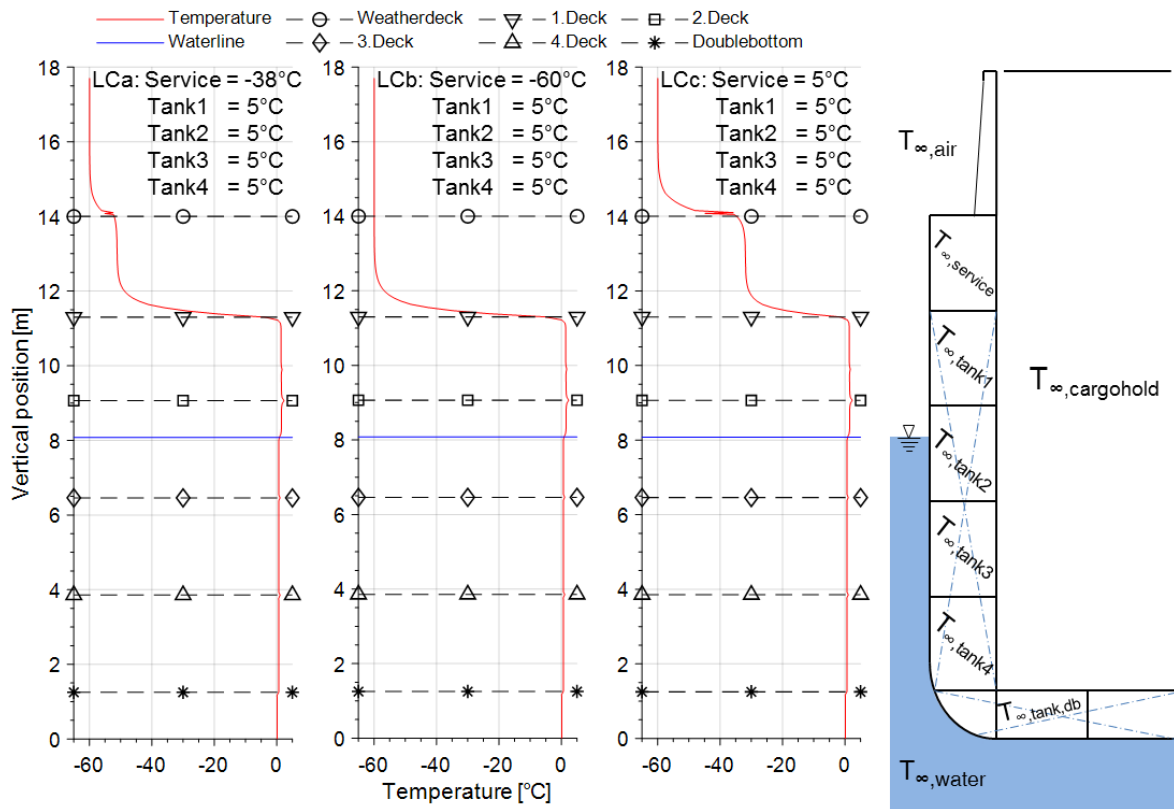


Fig.6: Temperature distribution in the outer shell plating for the load cases LCa, LCb and LCc

While the temperature is at 0 °C below the waterline and even above in the area of the filled side tanks above the waterline, it decreases very quickly in the area of the service corridor and finally reaches the ambient temperature of -60 °C. The influence of the ambient temperature in the service corridor on the temperature distribution can also be clearly seen in this case.

By comparison, Figure 7 clearly shows that when the side tanks are empty, the temperature in the structure directly above the waterline begins to drop rapidly. In the load cases LCd and LCe, no difference in the temperature distributions can be found due to the low temperature difference in the service corridor. Due to the significantly higher temperature in the service corridor, load case LCf shows at first glance a significantly different behaviour. However, significant deviations only occur more than one meter above the waterline and thus outside the collision area.

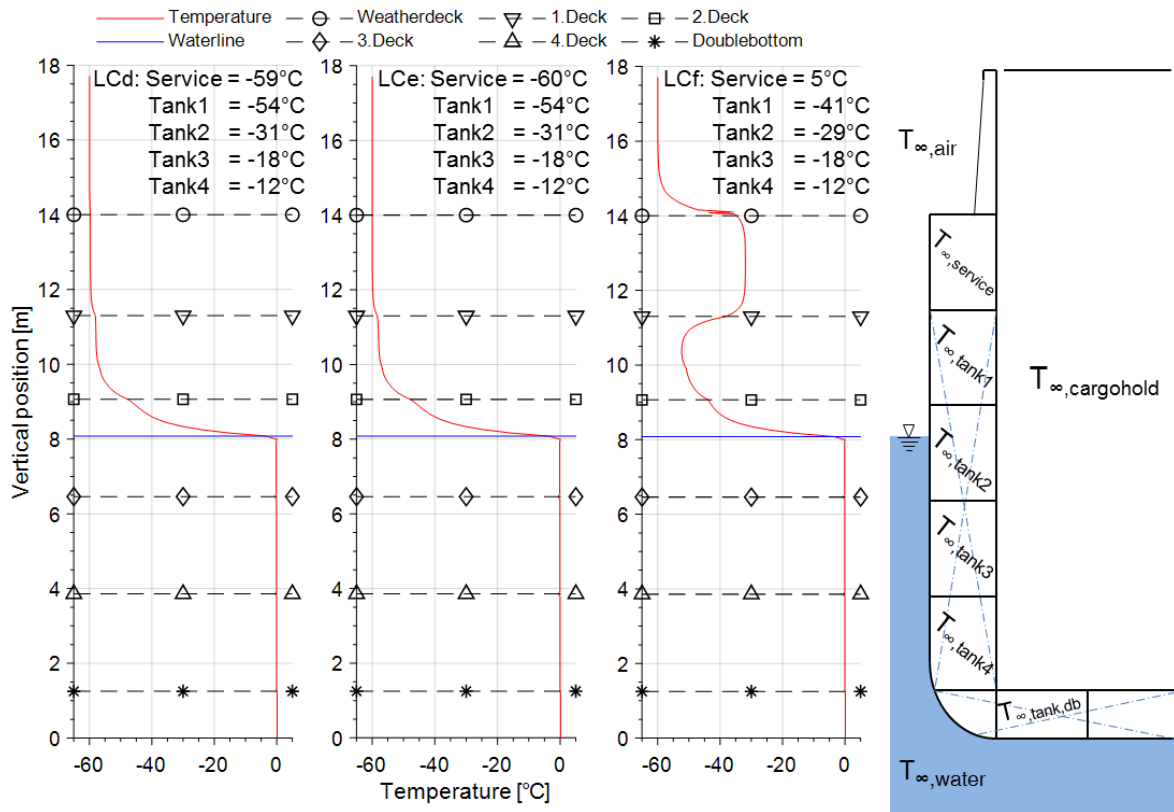


Fig.7: Temperature distribution in the outer shell plating for the load cases LCd, LCe and LCf

From these results, average temperatures for the collision area are derived for each load case, see Table 5. The height of the collision area is defined as the height above which the ship structure is loaded by the collision. This is determined by a collision simulation carried out in advance with the material data for the usual design temperature of 20 °C.

Table 5: Average temperatures for the collision area

Load case	Structure temperature
LCa	1 °C
LCb	1 °C
LCC	1 °C
LCd	-17 °C
LCe	-17 °C
LCf	-16 °C

The load cases LCa to LCc with filled side tanks all have an average temperature of 1 °C. For the load cases with empty side tanks the lowest temperature is -17 °C for load case LCd and LCe. The results show that load cases with filled side tanks can be neglected. But also load cases with empty tanks lead to structural temperatures in the area of the waterline which are clearly above the ambient air temperature.

In the absence of data for a corresponding material curve, the structural temperature for the subsequent collision simulation is approximated by a material curve for -20 °C. A further simulation is carried out under the assumption that the structure reaches the ambient temperature of -60 °C. This could be seen as the worst case scenario.

Figure 8 shows the maximum reaction forces occurring and the permanent deflections after the collision in normalized form. The results of the collision simulation with an assumed structural temperature of 20 °C serve as reference values.

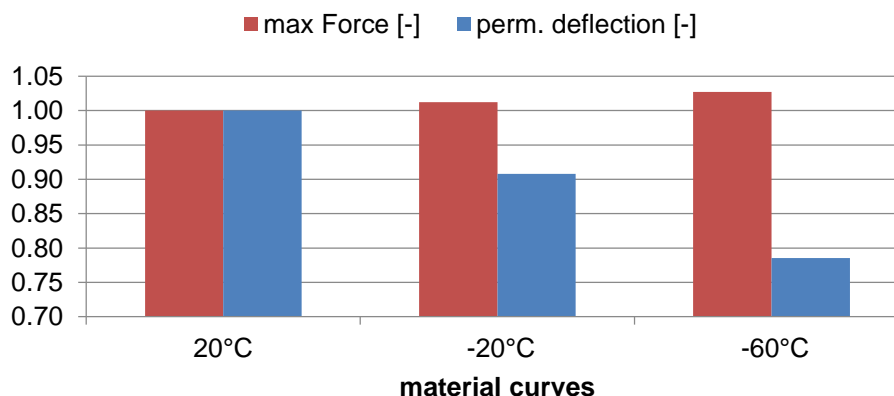


Fig.8: Reaction forces and permanent deflections

As the temperature decreases, the permanent deflection also decreases by about 10 % at -20 °C and even more than 20 % at -60 °C. At the same time, the increased stiffness of the structure leads to a slight increase in the reaction forces. On the one hand, the results show that neglecting the structural temperature leads to a conservative overestimation of the permanent deflection. On the other hand, the consideration of extreme values leads to an underestimation of the permanent deflection because the structure is assumed to be too stiff.

## 6 Conclusion and outlook

The simplified consideration of an averaged structural temperature for the determination of suitable material curves for modelling nonlinear plastic material behaviour clearly indicates the influence of temperature on the structural response in case of collisions. However, it also becomes clear that neglecting the temperature effects with regard to the structural response leads to conservative results. Nevertheless, a large temperature gradient over the height of the structure, especially in the waterline area, is observable. Therefore it would be desirable to use a temperature-dependent material model in the mechanical analysis instead of the presented averaged approach and to couple it directly with the thermal analysis to consider a more accurate resolution of the temperature distribution

In addition to the temperature effects, the dynamic material behaviour in the form of, for example, strain rate-dependent material curves should also be taken into account for collision simulations.

A possibility for future work to combine both effects of temperature and strain rate could be the use of the material law `*MAT_TABULATED_JOHNSON_COOK`, which allows the input of tabulated strain rate dependent and temperature dependent material curves.

Furthermore, it is desirable to include effects from wind, waves and currents in the analysis, as these could have a strong influence on the thermal boundary conditions, since both the relative velocities and the wetted area change as a result.

## 7 Summary

The determination of the structural temperature distribution of a ship cross-section and a collision scenario with a representative ice floe are presented. It is shown that the temperature of the ship's structure in the area of the waterline is clearly above the temperature of the surrounding air. The resulting structural response decreases with decreasing temperature. This leads to the conclusion that neglecting the influence of temperature and assuming a common ambient and structural temperature of 20 °C leads to an inaccurate but conservative result. On the other hand, the assumption of the extreme temperature of -60 °C as the structural temperature leads to an underestimation of the structural response.

## 8 Acknowledgements

We acknowledge the financial support of the Lloyd's Register Foundation within the "Recommended practice of scenario based risk management for polar waters". Lloyd's Register Foundation helps to protect life and property by supporting engineering-related education, public engagement and the application of research. It is stated that all funders are not responsible for any of the content of this publication.

## 9 References

- [1] V.-G. Schulze, "Arktisstrategien Überblick 2017," 2017. [Online] Available: <http://www.arctic-office.de/im-fokus/arktisstrategien-ueberblick/>. Accessed on: Oct. 25 2017.
- [2] S. Hänninen, *Incidents and accidents in winter navigation in the Baltic Sea, winter 2002-2003*. [Helsinki], [Tukholma]: Finnish Maritime Administration; Swedish Maritime Administration, 2005.
- [3] P. Kujala, "Damage statistics of ice-strengthened ships in the Baltic Sea 1984-1987," Helsinki University of Technology, Espoo, 1991.
- [4] J. K. Paik, K. J. Kim, J. H. Lee, B. G. Jung, and S. J. Kim, "Test database of the mechanical properties of mild, high-tensile and stainless steel and aluminium alloy associated with cold temperatures and strain rates," *Ships and Offshore Structures*, vol. 12, no. sup1, S230-S256, 2017.
- [5] DNV GL SE, *Rules for Classification and Construction, I Ship Technology, Part 1 - Seagoing Ships*, 2014.
- [6] American Bureau of Shipping (ABS), *Guide for Vessels Operating in low Temperature Environments*, 2016.
- [7] C. Emerson and G. Lahn, *Arctic Opening: Opportunity and Risk in the High North*. London, UK: Chatham House – Lloyd's, 2012.
- [8] Alfred-Wegener-Institut Helmholtz-Zentrum für Polar- und Meeresforschung, *Gefrierprozess von Meereis*. [Online] Available: <https://www.meereisportal.de/meereiswissen/was-ist-meereis/entstehung-von-meereis/gefrierprozess-von-meereis/>. Accessed on: Apr. 13 2019.
- [9] W. Fricke, *Vorlesungen zur Schiffskonstruktion (Bd.3)*. Hamburg, 2017.
- [10] L. Hoffmann and L. Müller, "Eisbelastung auf Vorschiff und Düsen von Forschungsschiff "Polarstern"," in *Jahrbuch der Schiffbautechnischen Gesellschaft*, 1985.
- [11] IMO, *MSC.1/Circ.1519 Guidance on Methodologies for Assessing Operational Capabilities and Limitations in Ice*, 2016.
- [12] K.-H. Grote and J. Feldhusen, *Dubbel: Taschenbuch für den Maschinenbau*. Berlin, Heidelberg: Springer Berlin Heidelberg, 2014.
- [13] W. Henschke, Ed., *Schiffbautechnisches Handbuch (Bd. 1; [Schiffstheorie - Widerstand, Propulsion und Steuern - Schiffsfestigkeit])*, 2nd ed. Berlin: Verl. Technik, 1966.
- [14] D. K. Perovich and K. F. Jones, "The seasonal evolution of sea ice floe size distribution," *J. Geophys. Res. Oceans*, vol. 119, no. 12, pp. 8767–8777, 2014.
- [15] D. A. Rothrock and A. S. Thorndike, "Measuring the sea ice floe size distribution," *J. Geophys. Res.*, vol. 89, no. C4, p. 6477, 1984.
- [16] T. Toyota, C. Haas, and T. Tamura, "Size distribution and shape properties of relatively small sea-ice floes in the Antarctic marginal ice zone in late winter," *Deep Sea Research Part II: Topical Studies in Oceanography*, vol. 58, no. 9-10, pp. 1182–1193, 2011.
- [17] T. Toyota, S. Takatsuji, and M. Nakayama, "Characteristics of sea ice floe size distribution in the seasonal ice zone," *Geophys. Res. Lett.*, vol. 33, no. 2, p. 1017, 2006.
- [18] G. W. Timco and R.M.W. Frederking, "A review of sea ice density," *Cold Regions Science and Technology*, vol. 24, no. 1, pp. 1–6, <http://www.sciencedirect.com/science/article/pii/0165232X9500007X>, 1996.
- [19] TraFi, *Ice Class Regulations and the Application Thereof (Finnish-Swedish Ice Class Rules)*, 2010.

- [20] LSTC, *LS-DYNA Theory Manual*, 2017th ed. Livermore, Calif.: Livermore Software Technology Corp, 2017.
- [21] Verein Deutscher Ingenieure; VDI-Gesellschaft Verfahrenstechnik und Chemieingenieurwesen, *VDI-Wärmeatlas: Mit 320 Tabellen*, 11th ed. Berlin: Springer Vieweg, 2013.
- [22] H. Herwig and A. Moschallski, *Wärmeübertragung*. Wiesbaden: Vieweg+Teubner, 2009.
- [23] K.-A. Reckling, *Theory of plasticity and their application to strength problems (translated from German language)*. Berlin, Heidelberg: Springer, 1967.
- [24] J. Kubiczek, K. Burchard, S. Ehlers, and M. SchötteIndreyer, "Material relationship identification for finite element analysis at intermediate strain rates using optical measurements," in *Progress in the Analysis and Design of Marine Structures*, Lisbon, Portugal, 2017, pp. 459–468.
- [25] G. D. Ashton, *River and lake ice engineering*. Littleton, Colo., U.S.A.: Water Resources Publications, 1986.
- [26] Z. Liu, J. Amdahl, and S. Løset, "Plasticity based material modelling of ice and its application to ship–iceberg impacts," *Cold Regions Science and Technology*, vol. 65, no. 3, pp. 326–334, 2011.
- [27] A. Derradji-Aouat, "Multi-surface failure criterion for saline ice in the brittle regime," *Cold Regions Science and Technology*, vol. 36, no. 1-3, pp. 47–70, 2003.